IOP Publishing Bioinspiration & Biomimetics
Bioinsp. Biomim. **4** (2009) 046003 (7pp) doi:10.1088/1748-3182/4/4/046003

Power distribution in the hovering flight of the hawk moth *Manduca sexta*

Liang Zhao and Xinyan Deng[1]

School of Mechanical Engineering, Purdue University, 500 Allison Rd., Chaffee Hall, West Lafayette, IN 47907, USA

E-mail: xdeng@purdue.edu

Received 22 April 2009
Accepted for publication 26 October 2009
Published 17 November 2009
Online at stacks.iop.org/BB/4/046003

Abstract
We investigated inertial and aerodynamic power consumption during hovering flight of the hawk moth *Manduca sexta*. The aerodynamic power was estimated based on the aerodynamic forces and torques measured on model hawk-moth wings and hovering kinematics. The inertial power was estimated based on the measured wing mass distribution and hovering kinematics. The results suggest that wing inertial power (without consideration of muscle efficiency and elastic energy storage) consumes about half of the total power expenditure. Wing areal mass density was measured to decrease sharply from the leading edge toward the trailing edge and from the wing base to the wing tip. Such a structural property helps to minimize the wing moment of inertia given a fixed amount of mass. We measured the aerodynamic forces on the rigid and flexible wings, which were made to approximate the flexural stiffness (EI) distribution and deformation of moth wings. It has been found that wings with the characteristic spanwise and chordwise decreasing EI (and mass density) are beneficial for power efficiency while generating aerodynamic forces comparative to rigid wings. Furthermore, negative work to aid pitching in stroke reversals from aerodynamic forces was found, and it showed that the aerodynamic force contributes partially to passive pitching of the wing

(Some figures in this article are in colour only in the electronic version)

1. Introduction

Power consumption in insect flight has been studied using numerical and experimental methods. Numerical methods were adopted to investigate the power consumption of the bumblebee, fruit fly and hawk moth (Wu and Sun 2005, Sun and Du 2003, Sun and Wu 2003, Liu and Aono 2009, Liu 2009). The results suggested that inertial power is important for large insects. Furthermore, the inertial power on insect wings was proposed to be the cause of wing pitching and deformations (Ennos 1988, Combes and Daniel 2002). In the previous study, the relative ratio of aerodynamic and inertia powers is important to the flight efficiency as the kinematics change (Usherwood 2009). And given the kinematics, the wing morphology and wing property in themselves can cause substantial variance in the inertial power consumption. Usually, the estimation of inertial power consumption has been based on the assumption that the wing moment of inertia is uniformly distributed across the wing surface (Sun and Tang 2002) or simplified to one-dimensional (Sun and Du 2003, Wu and Sun 2004, Bergou *et al* 2007, Willmott and Ellington 1997b, Ellington 1984, Liu and Aono 2009, Liu 2009). Experimental studies on hawk-moth wings were performed by changing the fixed angle of wing attack in a wind tunnel and measuring the steady-state forces (Willmott and Ellington 1997a). The resulting aerodynamic power was calculated as the power needed to move the wing to its maximum speed, using a one-dimensional wing moment of inertia (Willmott and Ellington 1997a, 1997b). Digital particle image velocimetry was used to measure the instantaneous downwash distribution, the middownstroke of a tethered desert locust and thus derive the correction factor for the actuator disc models of insect flight (Bomphrey *et al* 2006). In some studies, the aerodynamic forces were estimated via a quasi-steady model of a thin

[1] Author to whom any correspondence should be addressed.

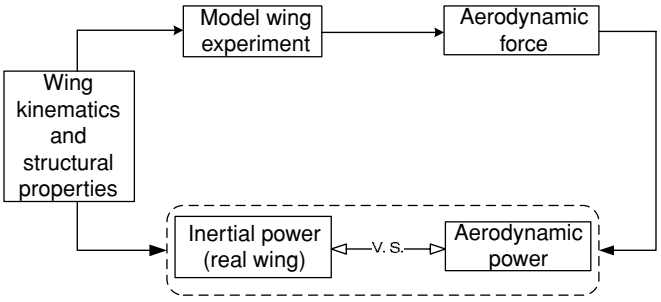

Figure 1. The combined analytical and experimental method to estimate the power consumption by hawk-moth wings.

plate interacting with the surrounding fluid (Berman and Wang 2007). Furthermore, the aerodynamic forces were estimated based on rigid wings, until recently when numerical research on flexible insect wings appeared (Zheng *et al* 2009).

In this study, we used combined experimental and analytical methods to investigate the aerodynamic and inertial power consumption by hawk moth *Manduca sexta* wings during hovering. We measured the aerodynamic forces on model robotic wings in fluids with matching Reynolds number, approximating wing flexural stiffness distribution and wing flexion patterns. The resulting aerodynamic forces were then scaled back to those on the real insects. The aerodynamic power was calculated based on wing kinematics and aerodynamic forces. We calculated the wing inertial power based on measured mass distribution and wing kinematics. The relative amount of inertial and aerodynamics power reveals the energy expenditure during hovering flight. An overview of our method is shown in figure 1.

In *Lepidoptera*, which include *Manduca* and most other moths, forewings and hindwings are mechanically coupled and flap in synchrony. However, flapping flight is driven primarily by actuation of the forewings. Hindwings were found to be unnecessary for normal flight and useful only for evasive flight (Jantzen and Eisner 2008). Compared to the forewing, the hindwing is smaller, lighter, much more flexible and closer to the wing base. Its contribution to the aerodynamic and inertial power is negligible compared to those by the forewings, also shown in this study (insection 4). Therefore, we will focus most of our analysis on the forewing.

2. Materials and methods

2.1. Experimental setup

We constructed a dynamically scaled mechanical flapper to measure aerodynamic forces on flapping wings (figure 2(*A*)). This flapper device is a slightly modified version of that described in Dickinson *et al* (1999), and unless otherwise mentioned, this paper follows the conventions and nomenclature of Sane and Dickinson (2001). The tests were conducted in light and clear oil. The driveshafts were powered by 16 mm, 0.3 Nm torque dc brush motors equipped with gear heads to reduce speed and magnetic encoders, thus providing kinematic feedback to ensure motion fidelity. The motors were driven along kinematic patterns provided by a custom MATLAB Simulink program with WinCon software. We used proportional-integral-derivative (PID) controllers to run the motors with a precision of 0.1°. More details on the experimental apparatus were described in Zhao *et al* 2009a, 2009b). The Reynolds number for our experiments was calculated at about 3000 using the equation

$$\bar{R}e = \frac{\bar{b}\bar{U}_t}{\nu} = \frac{4\theta R^2 n}{\nu(AR)}, \tag{1}$$

where $\bar{b}$ is the mean cord length, $\bar{U}_t$ is the mean wing-tip velocity, AR is the aspect ratio, n is the wing-beat frequency, R is the wing length, θ is the wing-beat amplitude (peak-to-peak in radians) and ν is the kinematic viscosity of the fluid (Ellington 1984). This Reynolds number is common for the hawk moth *Manduca sexta* in hover and was adopted in previous research (Ellington *et al* 1996, Usherwood and Ellington 2002, Willmott and Ellington 1997b).

2.2. Wing kinematics

Hovering wing kinematics was provided by Ty Hedrick with unpublished flight data of the hovering hawk moth *Manduca sexta* (figure 3). The wing kinematics were captured using high-speed video cameras and processed with a customized software package (Hedrick 2008). Note that the results represent the rigid part of the forewings.

2.3. Force measurement

The instantaneous forces on the model wings were measured using a six-component force balance (ATI NANO-17, Apex, NC). To derive the nondimensional force coefficients, we followed the conventions of Ellington (1984) and Dickinson *et al* (1999). The equation used to derive the lift and drag force coefficients was

$$C_F = \frac{F}{\frac{1}{2}\rho U_t^2 S_1 \cdot \hat{r}_2^2(S)}, \tag{2}$$

where ρ is the density of fluid, U_t is the path velocity of wing tip, and F is the lift (L), drag (D), or net force (N). In all the experiments described here, the area S_1 of each forewing is 5600 mm^2 and $\hat{r}_2^2(S)$, the nondimensional second moment of area, is 0.5.

Based on the force coefficients, the forces on the real insect wing are calculated (Zhao *et al* 2006) as

$$F_r = \tfrac{1}{2}\rho_a U_r^2 S_r \cdot \hat{r}_2^2(S_r) \cdot C_F, \tag{3}$$

where F_r is the estimated forces on real hawk-moth wing, ρ_a is the air density, U_r is the wing-tip velocity, S_r is the wing area, $\hat{r}_2^2(S_r)$ is the nondimensional second moment of wing area and C_F is force coefficients.

2.4. Measuring the areal distribution of wing mass density

The areal density of the Manduca wings were measured based on freshly cut left and right wings of two moths (*Manduca sexta*, about 1.5 g, female). The wings were cut into small parallel slices along spanwise and chordwise directions, and the area and mass for each slice were measured. The measurements provide the discrete mass–density distribution. We then used mathematical fitting functions to obtain an approximate continuous wing mass–density distribution function.

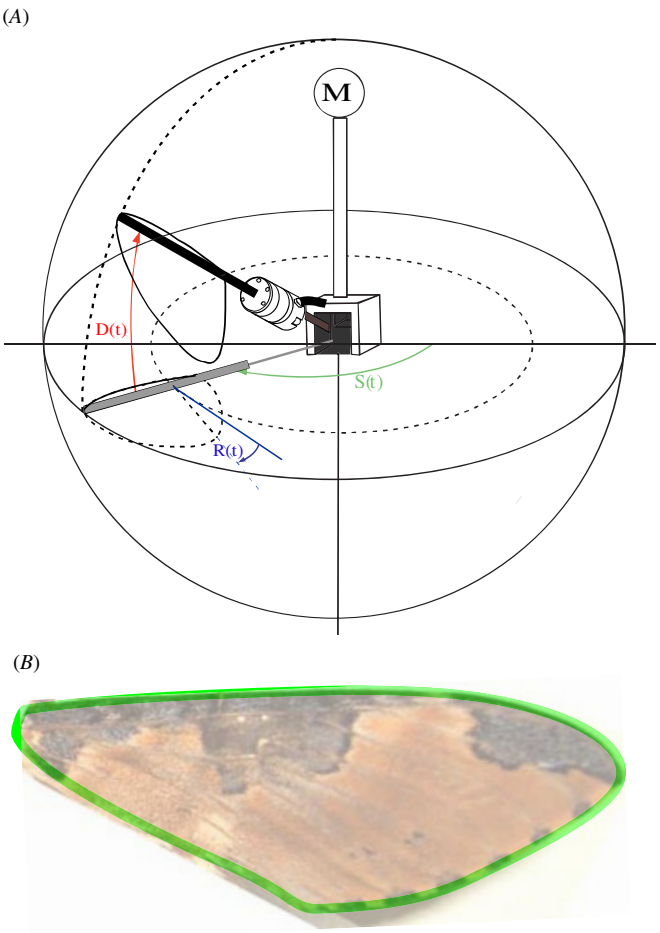

Figure 2. The experimental setup. (*A*) The flapper used for the force measurement experiments and (*B*) shape of a model forewing (made of PETG; thickness 1.5 mm, green) and a *Manduca* forewing (48 mm span). Note, the size of the two have been rescaled.

2.5. Aerodynamic power calculation

Given the kinematics and forces on the wing, the aerodynamic power consumption can be calculated using the following equation:

$$P = \begin{bmatrix} M_S & M_D & M_R \end{bmatrix} \begin{bmatrix} \frac{\mathrm{d}S_e}{\mathrm{d}t} & \frac{\mathrm{d}D_e}{\mathrm{d}t} & \frac{\mathrm{d}R_e}{\mathrm{d}t} \end{bmatrix}^T, \tag{4}$$

where M_S, M_D and M_R are the aerodynamic torques along the principle axes of stroke, deviation and rotation of the wing (figure 2(*A*)). $\mathrm{d}S_e/\mathrm{d}t$, $\mathrm{d}D_e/\mathrm{d}t$ and $\mathrm{d}R_e/\mathrm{d}t$ are angular velocities of stroke, deviation and rotation angles, which all were from the encoder outputs. The backlash of gears is negligible after calibration, and the encoder data can accurately represent the real angles of the wing after proper conversion. Furthermore, to reduce the noise, we process the signals using a low pass filter.

Traditionally, the wing inertial power was derived based on a simplified one-dimensional wing moment of inertia, or an evenly distributed chordwise wing mass. Two-dimensional moments of inertia and mass distribution were rarely used because of their complexity. To derive the wing inertial power, we integrated the kinetic energy of the wing along the wing area, then differentiated it by time to obtain the inertial power matrix as a function of time (equation 5).

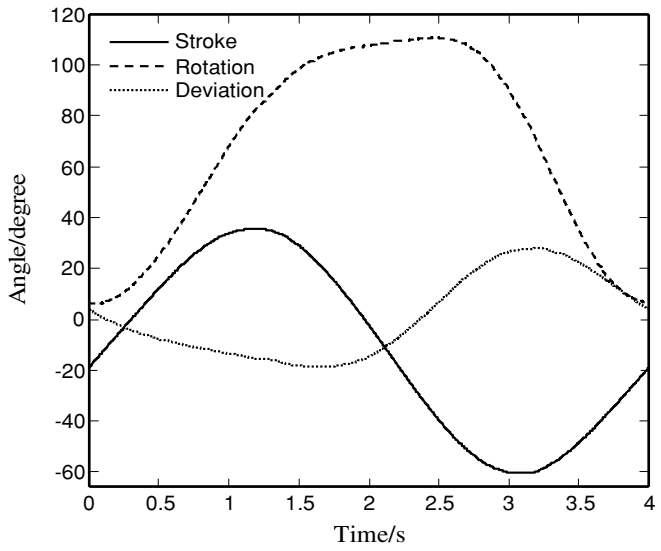

Figure 3. Wing kinematics of *Manduca sexta* in hover.

$$E_k(t) = \int \frac{1}{2}\rho(c,r)V^2(c,r,t)\,\mathrm{d}S, \tag{5a}$$

$$P(t) = \frac{\mathrm{d}E_k(t)}{\mathrm{d}t}. \tag{5b}$$

Here E_k is the kinetic energy, $\mathrm{d}S$ is the area of a square located at distance c (chordwise) from the leading edge and at distance r (spanwise) from the wing base, $\rho(c,r)$, the areal mass density and $V(c,r,t)$, the local wing velocity.

3. Results

3.1. Wing areal mass–density distribution

Figure 4 shows the one-dimensional mass distribution along the spanwise and chordwise directions. The areal mass density decreases sharply from the wing base toward the wing tip and from the leading edge to the trailing edge. The mass was distributed evenly neither by length nor by area. The wing tip and trailing edge are light and flexible and are capable of deforming. The wing base and leading edge are relatively stronger and more rigid.

3.2. Aerodynamics and inertial power consumption for the Manduca *wings*

The aerodynamics and inertial power of the forewing is shown in figure 5. The inertial force was calculated based on wing kinematics and mass distribution. The aerodynamic forces were measured using rigid model wings, then scaled to the forces on insect wings. It shows that the amplitude of the aerodynamic power is about twice that of the inertial power. However, the mean values (11.8 mW versus 9.8 mW) are close, indicating comparable power expenditure on aerodynamics and inertia. As seen in figure 5, positive work is required for the motion of the wing. Meanwhile, negative aerodynamics power appears at the stroke reversal for a certain amount of passive pitching of the wings.

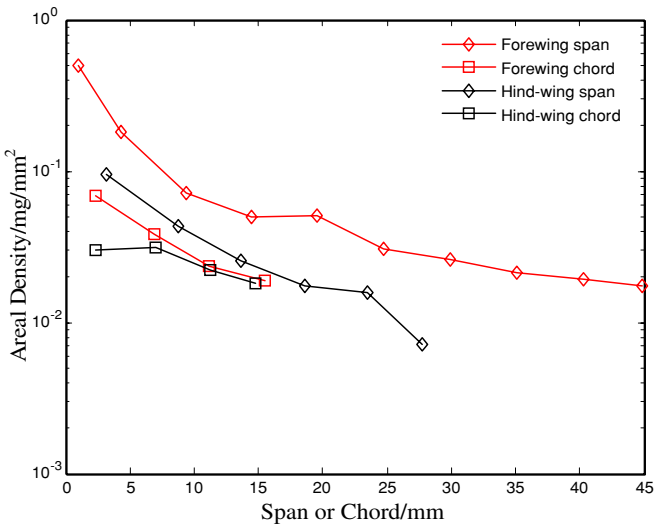

Figure 4. Chordwise and spanwise distributions of wing areal mass density. The *x*-axis is the distance along the chordwise or spanwise direction from the wing leading edge or wing base. The *y*-axis is areal mass density in the log scale.

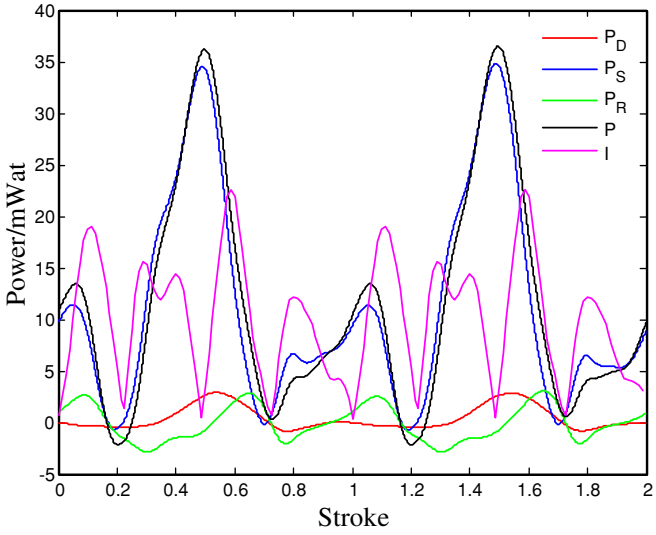

Figure 5. Aerodynamics and inertial power consumption. The subscripts D, R and S are for deviation, rotation and stroke angles. *P* and *I* denote total aerodynamics and inertial power.

In our experiments, the forewings have a relative power-to-weight ratio (P/W) of 16.4 (inertial) and 19.7 (aerodynamics) mW g^{-1}. The total forewing P/W is 36.1 mW g^{-1}. Since the hindwing contributes much less to total power, the total power is within the range of the previous study: the combined inertial and aerodynamic power of the hawk moth can be as much as 18–61 mW g^{-1} (Sun and Du 2003). In a separate study, the mean aerodynamic and inertial powers are 39.5 mW g^{-1} and 27.25 mW g^{-1}, respectively, for the hawk moth (Liu and Aono 2009), close to our results and also to Sun's. The minor differences may be because aerodynamic and inertia powers were derived by being based on different methods. For aerodynamics, Liu and Aono used the computational fluid dynamic (CFD) methods, but we used an experimental method; for inertial power, we have different assumptions regarding the moment of inertia on the wings.

4. Discussions

4.1. Power distribution: inertial and aerodynamic

The wing inertia can dominate wing deformation (Combes and Daniel 2003c, Mountcastle and Daniel 2009, Berman and Wang 2007). However, the inertial power consumption is nonviable regardless of such aerodynamic contributions (Usherwood and Ellington 2002, Berman and Wang 2007). For small insects (for example, the fruit fly) and for medium and large insects with relatively low wing-beat frequency (such as the crane fly, lady bird and hawk moth), power is mostly spent on aerodynamics. For medium and large insects with relatively high wing-beat frequency (such as the hoverfly, drone fly, honeybee and bumblebee), power is mostly spent to overcome wing inertia (Sun and Du 2003, Sun and Wu 2003).

Our results show that the inertial power has a mean value comparable to that of aerodynamic power. The insects, different from the rigid wing man-made aerial vehicles, must exert considerable energy to overcome wing inertia. The high maneuverability of flapping flight (Dudley 2002), compared to rigid- or rotary-wing aircraft, is at the cost of high inertial power consumption. Meanwhile, the inertial power could also contribute to other factors, such as wing deformation.

4.2. Aerodynamics: flexible versus rigid wings

Wing compliance may affect overall flow in the hawk moth (Mountcastle and Daniel 2009), and the aerodynamics will be affected by the flow-field changes. Force measurement based on model rigid wings is an approximation of the aerodynamic force, since the effect of wing deformation may not be negligible. To compare the results, we used a model wing that approximate the real wing deformation and measured its aerodynamic forces and torques. We adopted the structure of decreasing flexural stiffness (EI) along the spanwise and chordwise directions based on measurements of real insect wings (Combes and Daniel 2003a, 2003b). Four pieces of polymer materials were properly aligned and attached to approximate the EI distribution (figure 6). They were PETG 0.06″, POLYCARB 0.015″, POLYES 0.005″, and POLYES 0.002″ (figure 6(*A*)), in the order of deceasing EI. The thickness, EI, and shape alignments of the materials were tuned to result in deformation similar to that on moth wings. Matching the deformation can help us mimic the real flow around the insect wing by matching the force vector direction and the vortex structures. In figure 6(*A*), EI values at the four asterisks on the model wing decreased exponentially from left to right. Such discrete arrangements of decreasing EI would be an acceptable approximation of the continuous decreasing EI of the hawk-moth wings, based on the wing's flexural stiffness properties.

The deformation was captured in motion as shown in figure 6(*B*), where similar deformation on leading edges between the model wing and the *Manduca* wing was shown at

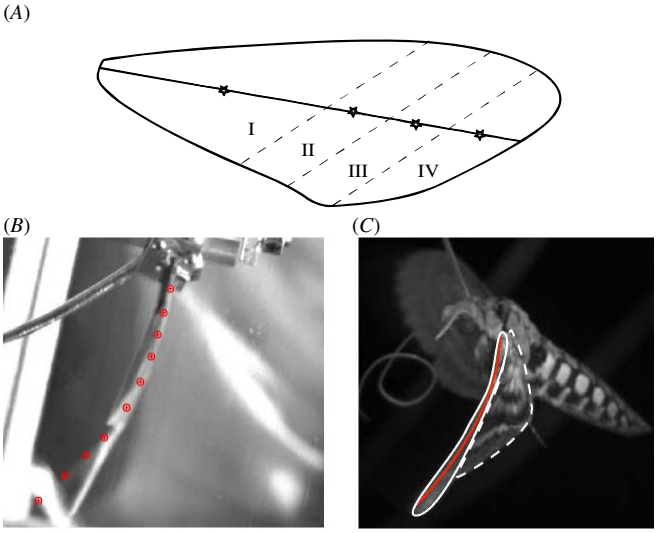

Figure 6. Flexible model wing and deformation in flight. (*A*) The wing structure of the flexible model wing. The bending stiffness at the four sections follows the exponential decreasing EI starting from the base, (*B*) deflection of the model wing during experiments; red dots denote the leading edge and (*C*) *Manduca* wing deflection at the same wing position as B; the red line denotes the leading edge. The dashed line is the contour of the hindwing and the solid white line is the contour of the forewing.

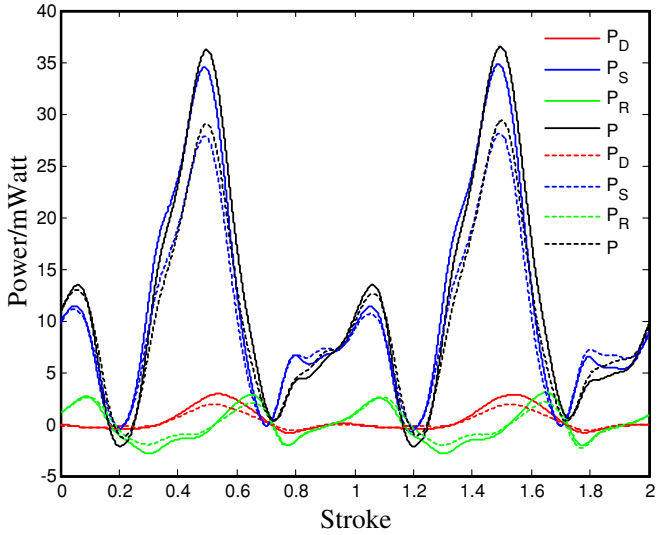

Figure 7. Aerodynamic power on flexible and rigid wings. The subscripts D, R and S are for deviation, rotation and stroke power, respectively. *P* denotes total aerodynamic power. Dashed lines represent power on flexible wings and solid lines on rigid ones.

the time of upstroke just passing the horizontal plane. Here we neglect the slight asymmetry between the dorsal and ventral EI, though the asymmetry in dorsal/ventral flexural stiffness was found on *Manduca* wings (Combes and Daniel 2003b) and on other insects (Wootton *et al* 2000; Wootton 1993, Steppan 2000). The power distribution of a deformable wing is compared in figure 7 with that of a rigid wing. For the flexible model wing in this experiment, aerodynamic force is slightly lower than the rigid wing, resulting in a reduction of about 20% in aerodynamic power.

4.3. Passive pitching

During wing pitch reversal, the rapid change of angle of attack can be caused by the fluid force and the inertial force. A study using a quasi-steady method showed that the pitching (rotation) can be passive, since the rotational power is negative (Bergou *et al* 2007). Our results, which were designed to bear span- and chordwise wing characters, also show the negative aerodynamic power in pitching. At stroke reversals (figure 8), the rotational powers were negative, and the wing pitching was caused by the fluid. For the other two degrees of freedom (stroke and deviation), the power was always positive and there was no passive motion caused by the fluid (figures 5 and 7). For wing pitching, despite negative power at stroke reversal, there are also positive powers at other instants. This is due to the active rotation of the wing.

4.4. Forces on the hindwing

To examine how much the hindwing contributes to aerodynamic force generation, the following experiments were performed. Three model hindwings were made with varying EIs. They were individually attached to the flexible forewing and driven at hovering kinematics. Compared with the forewings, the hindwings are smaller, lighter and closer to the body; they are also more flexible.

As a result, they produce much less aerodynamic force than the forewings do. The area of the hindwing is about 50% that of the forewing, but the hindwing produces less than 23% of the force of the forewing (figure 9).

When scaled on the real wing, the combined forewing and hindwing models produce almost the same amount of lift force as the real wing (equal to the body mass to balance the weight). Among them the polyest 0.002″ can generate a mean lift of 0.0144 N, which can balance the 1.47 g weight. On a side note, errors in matching the wing deformation pattern can be assured here because the lift difference between our model and the real insect wing is trivial compared to the total force. When rescaled to the insect wing, the rigid-wing model can produce a high lift of 1.81 g. It is much higher than the real body mass. With no consideration of the inertial power waste, the rigid model will be beneficial for the insect flight because it can produce much more lift force when the kinematics remain the same.

4.5. Implications for micro aerial vehicle wing design

The *Manduca* wing is flexible, light and effective in force generation. To make man-made flapping wing micro aerial vehicles, the wing mass distribution is a key factor to be considered. Consider a wing with uniform areal mass–density distribution which is adopted in some MAV wing designs with isotropic wings. Instead of the sharply decreasing areal mass–density from base to tip and from the leading edge to trailing edge, $\rho(c, r)$ in equation (5*a*) will be a constant. Given the same total mass, calculations suggest that the inertial power will be as high as 1.9 times of the wings with hawk moth mass–density distribution. On the other hand, wings made

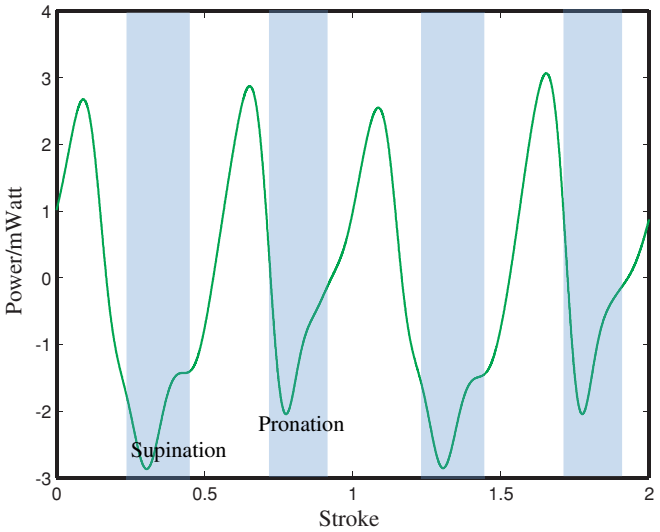

Figure 8. Wing rotational aerodynamic power. The shadowed area denotes pronation and supination, where negative aerodynamic power was found to aid wing pitching. Positive power during other instants reveals active rotation.

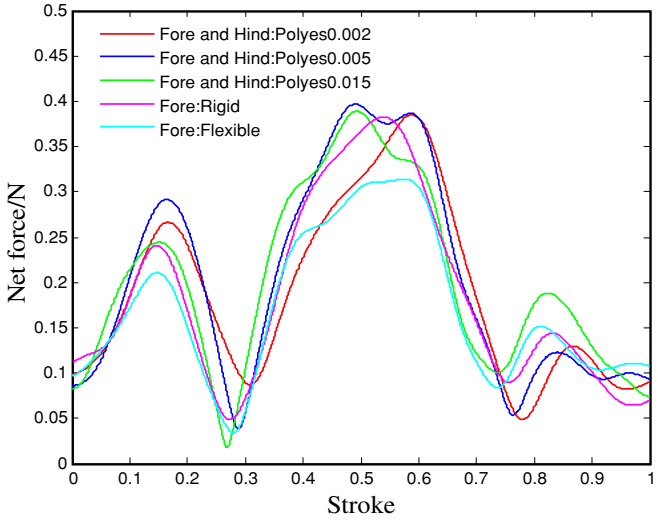

Figure 9. Aerodynamic forces on forewing only and forewing plus hindwing. Five models were used for force measurements. One is the rigid forewing and the other is the flexible forewing used in previous experiments. The remaining three wings consist of a forewing–hindwing pair using a flexible forewing of previous experiments and flexible hindwings made of polyester with thicknesses of 0.002″, 0.005″, and 0.015″ in the order of increasing EI.

of thin membrane reinforced by wing veins offer a solution to maintain the rigidity of the wing (for force generation) while keep it at low weight and inertia. Therefore, for engineering design of micro aerial vehicles to minimize the wing moment of inertia, structural properties such as wing veins and concentrating most mass close to wing base should be adopted since it reduces the inertial power while only cause small amount of reduction on aerodynamic forces.

5. Conclusion

We investigated the inertial and aerodynamic power consumptions in hovering flight of the hawk moth *Manduca sexta*. The aerodynamic power was estimated based on the aerodynamic forces and torques measured on model hawkmoth wings and hovering kinematics. The inertial power was estimated based on measured wing-mass distribution and hovering kinematics. The results suggest that wing inertial power (without consideration of muscle efficiency and elastic energy storage) consumes about half of the total power expenditure. Wing areal mass density was measured to decrease sharply from the leading edge toward the trailing edge and from the wing base to the wing tip. This structural property helps to minimize the wing moment of inertia given a fixed amount of mass. We measured the aerodynamic forces on rigid and flexible wings that were made to approximate the flexural stiffness (EI) distribution and the deformation of moth wings. It is found that wings with the characteristic spanwise and chordwise decreasing EI (and mass density) are beneficial for power efficiency, while generating comparative aerodynamic forces to rigid wings. Furthermore, negative work to aid pitching in stroke reversals from aerodynamic forces was found, and it showed that the aerodynamic force contributes partially to a passive pitching of the wing.

Acknowledgments

The authors thank Tyson Hedrick and Alice Robinson from the University of North Carolina for providing the Manduca hovering flight kinematics and wing mass distribution measurements. This work was supported in part by the National Science Foundation Award 0545931 to XD.

References

Bergou A J, Xu S and Wang Z J 2007 Passive wing pitch reversal in insect flight *J. Fluid Mech.* **591** 321–37

Berman G J and Wang Z J 2007 Energy-minimizing kinematics in hovering insect flight *J. Fluid Mech.* **582** 153–68

Bomphrey R J, Taylor G K, Lawson N J and Thomas A L 2006 Digital particle image velocimetry measurements of the downwash distribution of a desert locust *Schistocerca gregaria J. R. Soc. Interface* **3** 311–17

Combes S A and Daniel T L 2002 Flexible wings and fins: bending by inertial or fluid-dynamic forces? *Integr. Comput. Biol.* **42** 1044–26

Combes S A and Daniel T L 2003a Flexural stiffness in insect wings: I. Scaling and the influence of wing venation *J. Exp. Biol.* **206** 2979–87

Combes S A and Daniel T L 2003b Flexural stiffness in insect wings: II. Spatial distribution and dynamic wing bending *J. Exp. Biol.* **206** 2989–97

Combes S A and Daniel T L 2003c Into thin air: contributions of aerodynamic and inertial-elastic forces to wing bending in the hawkmoth *Manduca sexta J. Exp. Biol.* **206** 2999–3006

Dickinson M H, Lehmann F O and Sane S P 1999 Wing rotation and the aerodynamic basis of insect flight *Science* **284** 1954–60

Dudley R 2002 *The Biomechanics of Insect Flight: Form, Function, Evolution* (Princeton, NJ: Princeton University Press)

Ellington C P 1984 The aerodynamics of hovering insect flight: VI. Lift and power requirements *Phil. Trans. R. Soc. Lond.* **305** 145–81

Ellington C P, Vandenberg C, Willmott A P and Thomas A L R 1996 Leading-edge vortices in insect flight *Nature* **384** 626–30

Ennos A R 1988 The inertial cause of wing rotation in Diptera *J. Exp. Biol.* **140** 161–69

Hedrick T L 2008 Software techniques for two- and three-dimensional kinematic measurements of biological and biomimetic systems *Bioinsp. Biomim.* **3** 034001

Jantzen B and Eisner T 2008 Hind wings are unnecessary for flight but essential for execution of normal evasive flight in Lepidoptera *Proc. Natl Acad. Sci. USA* **105** 16636–40

Liu H 2009 Integrated modeling of insect flight: from morphology, kinematics to aerodynamics *J. Comput. Phys.* **228** 439–59

Liu H and Aono H 2009 Size effects on insect hovering aerodynamics: an integrated computational study *Bioinsp. Biomim.* **4** 15002

Mountcastle A M and Daniel T L 2009 Aerodynamic and functional consequences of wing compliance *Exp. Fluids* **46** 873–82

Steppan S J 2000 Flexural stiffness patterns of butterfly wings (*Papilionoidea*) *J. Res. Lepid.* **35** 61–77

Sun M and Du G 2003 Lift and power requirements of hovering insect flight *Acta Mech. Sin.* **19** 458–69

Sun M and Tang J 2002 Lift and power requirements of hovering flight in *Drosophila virilis J. Exp. Biol.* **205** 2413–27

Sun M and Wu J H 2003 Aerodynamic force generation and power requirements in forward flight in a fruit fly with modeled wing motion *J. Exp. Biol.* **206** 3065–83

Usherwood J R 2009 Inertia may limit efficiency of slow flapping flight, but mayflies show a strategy for reducing the power requirements of loiter *Bioinsp. Biomim.* **4** 015003

Usherwood J R and Ellington C P 2002 The aerodynamics of revolving wings: I. Model hawkmoth wings *J. Exp. Biol.* **205** 1547–64

Willmott A P and Ellington C P 1997a The mechanics of flight in the hawkmoth *Manduca sexta*: I. Kinematics of hovering and forward flight *J. Exp. Biol.* **200** 2705–22

Willmott A P and Ellington C P 1997b The mechanics of flight in the hawkmoth *Manduca sexta*: II. Aerodynamic consequences of kinematic and morphological variation *J. Exp. Biol.* **200** 2723–45

Wootton R J 1993 Leading edge section and asymmetric twisting in the wings of flying butterflies (*Insecta, Papilionoidea*) *J. Exp. Biol.* **180** 105–17

Wootton R J, Evans K E, Herbert R and Smith C W 2000 The hind wing of the desert locust (Schistocerca gregaria Forskal): I. Functional morphology and mode of operation *J. Exp. Biol.* **203** 2921–31

Wu J H and Sun M 2004 Unsteady aerodynamic forces of a flapping wing *J. Exp. Biol.* **207** 1137–50

Wu J H and Sun M 2005 Unsteady aerodynamic forces and power requirements of a bumblebee in forward flight *Acta Mech. Sin.* **21** 207–17

Zhao L, Huang Q, Deng X and Sane S 2009a Aerodynamic effects of flexibility in flapping wings *J. R. Soc. Interface* rsif.2009.0200v1 (published online 19 August 2009)

Zhao L, Huang Q, Deng X and Sane S 2009b The effect of chord-wise flexibility on the aerodynamic force generation of flapping wings: experimental studies *IEEE Int. Conf. on Robotics and Automation (Kobe, Japan)*

Zhao L, Jing J, Lu X Y and Yin X Z 2006 Measurements and analysis of force and moment of caudal fin model in C-start *Prog. Nat. Sci.* **16** 796–802

Zheng L, Wang X, Khan A, Vallance R and Mittal R 2009 A combined experimental-numerical study of the role of wing flexibility in insect flight *AIAA Aerospace Sciences Meeting Including The New Horizons Forum and Aerospace Exposition (Orlando, FL)*